




Generation of high-temporal-quality sub-two-cycle pulses by self-cleaning of spatiotemporal solitons in air-plasma channels

Litong Xu  and Tingting Xi *School of Physical Sciences, University of Chinese Academy of Sciences, Beijing 100049, China* (Received 16 October 2023; revised 6 March 2024; accepted 25 March 2024; published 11 April 2024)

The temporal sidelobes of few-cycle pulses seriously restrict their applications in ultrafast science. We propose a unique mechanism that enables the generation of sub-two-cycle pulses with a high temporal quality. A robust spatiotemporal soliton could be formed from pulse self-compression by modulating the dispersion of the air-plasma channel via the adjusted plasma density. The self-cleaning of the spatiotemporal soliton leads to the elimination of sidelobes in the temporal profile of the sub-two-cycle pulse. The required density of the preformed plasma for an arbitrary central wavelength from the near-infrared to midinfrared regime is predicted theoretically and confirmed by (3D+1) simulations.

DOI: [10.1103/PhysRevA.109.043513](https://doi.org/10.1103/PhysRevA.109.043513)

I. INTRODUCTION

Intense ultrashort pulses with durations down to a few optical cycles have been strongly demanded by ultrafast science and strong-field physics [1,2]. For instance, few-cycle pulses serve as important driving sources for generating ultraviolet radiation and isolated attosecond pulses [3,4]. Furthermore, in the field of laser-driven ion acceleration, intense few-cycle pulses show remarkable advantages in enhancing the efficiency and stability of the system [5,6]. Typically, few-cycle pulses can be generated by pulse compression of the supercontinuum based on nonlinear propagation in Kerr media [7–12]. Up to now, the pulse duration has entered the single-cycle regime [7] and the peak power has reached the terawatt level [8]. However, the temporal quality as another important characteristic has not been significantly improved. To be specific, high-peak-power few-cycle pulses, especially sub-two-cycle pulses, are usually accompanied by one or several temporal sidelobes, which are very unfavorable for ultrafast applications [3]. The temporal sidelobes are formed mainly due to the uncompensated spectral phase induced by high-order nonlinear effects [9,13]. Despite the quality improving approaches including additional third-order dispersion compensation [10] and the pressure gradient [11], their parameter sensitivity makes it still a challenge to obtain intense few-cycle pulses with a high temporal quality.

Recall the self-cleaning of the spatial distribution in filamentation, where a central peak is formed by the Kerr self-focusing, and the spatial sidelobes are diffracted to the energy reservoir [14]. Therefore, we expect to also observe temporal self-cleaning if a long-distance spatiotemporal soliton (STS) can be formed during filamentation. We consider using the air with a preformed uniform plasma channel as the medium to support the formation of STS, because the controllable negative dispersion via changing electron density is very beneficial for the temporal control of pulses [15].

In this paper we propose a unique scheme to improve the temporal quality of few-cycle pulses by the self-cleaning of STS in air-plasma channels. In our scheme, a long-distance STS can be formed by self-compression of the femtosecond laser pulse in the air-plasma channel, where the required electron density is estimated theoretically and confirmed by simulation results. The robust propagation of STS leads to pulse self-cleaning, which eliminates sidelobes and significantly improves the temporal quality of the pulse. Notably, this scheme can be used to generate sub-two-cycle pulses with different wavelengths, which will greatly favor wavelength-dependent applications in ultrafast science.

II. MODEL

To form a long-distance STS with ultrashort duration, two conditions are necessary. First, the spectrum is superbroadened so that it can support a sub-two-cycle or even single-cycle pulse. Second, the nonlinear length should be close to the dispersion length for a stable temporal soliton, while spatially the beamwidth may be maintained by the dynamic balance of Kerr focusing and plasma defocusing as a feature of filamentation. To satisfy the two conditions, we first analyze the temporal evolution of the pulse. During the self-focusing stage of the laser pulse, the self-phase modulation dominates the temporal evolution, leading to a positively chirped pulse. When air ionization occurs with the increase of laser intensity, plasma defocusing becomes prominent, and the positively chirped pulse splits into two subpulses. The trailing subpulse has a higher frequency. The two subpulses will be further separated in a normally dispersive medium and will draw closer in a negatively dispersive medium. If the two subpulses could not coalesce, the leading subpulse will diffuse first, resulting in the weakening of an important part of the broadened spectrum. It may affect the temporal profile and duration of the obtained few-cycle pulse after the nonlinear propagation. Therefore, the divergence of the leading subpulse should be prevented, and the negative dispersion of the air-plasma channel should be strong enough to

*ttxi@ucas.ac.cn

drive the coalescence of the subpulses. We set the frequencies of the two subpulses to be ω_1 and ω_2 , with the frequency difference $\Delta\omega = \omega_2 - \omega_1$. After a propagation distance Δz , the decrease of the time interval of the subpulses is calculated by $\frac{\Delta z}{v_{g|\omega_2}} - \frac{\Delta z}{v_{g|\omega_1}} \approx k^{(2)}|_{\omega_0} \Delta\omega \Delta z$. Here, v_g is the group velocity, $k^{(2)}$ is the group-velocity dispersion (GVD) coefficient, and ω_0 is the central frequency of the laser pulse. This approximation is performed based on the definition of the GVD coefficient $k^{(2)} = \frac{d}{d\omega}(\frac{1}{v_g})$. In the preformed air-plasma channel, the group-velocity dispersion is contributed by air and plasma: $k^{(2)} = k_a^{(2)} + k_p^{(2)}$. Therefore, to merge the two subpulses with an initial time interval Δt , the GVD coefficient of the plasma should satisfy the following equation:

$$-(k_p^{(2)} + k_a^{(2)})\Delta\omega\Delta z = \Delta t. \quad (1)$$

Here, $k_p^{(2)}$ and $k_a^{(2)}$ are the GVD coefficients of the plasma and air, respectively. The frequency difference of the subpulses is supposed to be mainly induced by self-phase modulation, then it is estimated to be $\Delta\omega = 2.86B/\tau_0$ [16], where τ_0 is the initial pulse duration [full width at half maximum (FWHM)]. The nonlinear phase shift is taken to be $B = 2\pi$, when plasma defocusing becomes prominent and pulse splitting occurs [17]. To prevent the leading subpulse from diverging, the propagation distance required for the temporal coalescence should be shorter than the diffraction length of a single subpulse. This length can be roughly estimated by $\Delta z = 2\pi w_f^2/\lambda_0$, and is shorter than the length of filamentation that may include many focusing-defocusing cycles [18]. The radius of filament is $w_f = \lambda_0/\sqrt{8n_2 I_p}$, where λ_0 is the central wavelength and n_2 is the coefficient of nonlinear refractive index [19]. For simplicity, the clamping intensity is fixed at a typical value of $I_p = 60 \text{ TW/cm}^2$. The time interval Δt is assumed to be $\Delta t \approx 0.5\tau_0$. By applying this setting, we obtain the desired GVD coefficient induced by plasma:

$$k_p^{(2)} = -\frac{n_2 I_p \tau_0^2}{28.2\lambda_0} - k_a^{(2)}. \quad (2)$$

From Eq. (2) we can get the corresponding density ρ_p of the preformed plasma channel by $k_p^{(2)} = -1.58 \times 10^{-5} \lambda_0^3 \rho_p$ (fs^2/cm), with λ_0 and ρ_p in SI units [15]. We find that the estimated GVD coefficient can also fulfill the second condition, with the nonlinear length nearly equal to the dispersion length. Then we perform numerical studies on pulse self-compression in air-plasma channels to verify our analysis.

The propagation of femtosecond laser pulses in air with preformed uniform plasma channel can be described by the [three-dimensional (3D)] (3D+1) nonlinear envelope equation coupled with the electron density evolution equation [12], where the former governs the pulse envelope $\mathcal{E}(x, y, t, z)$ in the frame moving with the group velocity of central wavelength ($t \rightarrow t - z/v_g$). The coupled equations are given by

$$\frac{\partial \mathcal{E}}{\partial z} = \frac{i}{2k_0} T^{-1} \nabla_{\perp}^2 \mathcal{E} + i \frac{\omega_0}{c} n_2 T \int_{-\infty}^t \mathcal{R}(t-t') |\mathcal{E}(t')|^2 dt' \mathcal{E} + i \mathcal{D} \mathcal{E} - i \frac{k_0}{2\rho_{c0}} T^{-1} \rho \mathcal{E} - \frac{U_i W(|\mathcal{E}|)(\rho_{nt} - \rho)}{2|\mathcal{E}|^2} \mathcal{E} \quad (3)$$

$$\frac{\partial \rho}{\partial t} = W(|\mathcal{E}|)(\rho_{nt} - \rho_0 - \rho), \quad (4)$$

where z is the propagation distance, $k_0 = 2\pi/\lambda_0$ is the central wave number, $T = 1 + (i/\omega_0)\partial_t$, $\mathcal{D} = \sum_{n \geq 2} (k^{(n)}/n!) (i\partial_t)^n$, $k^{(n)} = \partial^n k / \partial \omega^n |_{\omega_0}$. The dispersion relation of the uniform air-plasma channel is $k(\omega) = k_a(\omega) - \rho_0 \omega / 2c \rho_c$. Here, $k_a(\omega)$ is the dispersion relation of air [20,21] and ρ_0 is the density of preformed plasma. The critical plasma density $\rho_c(\lambda) = 1.11 \times 10^9 / \lambda^2 \text{ cm}^{-3}$ is wavelength dependent, accounting for the negative dispersion, and $\rho_{c0} = \rho_c(\lambda_0)$. The ionization rate $W(|\mathcal{E}|)$ is calculated from the Perelomov-Popov-Terent'ev model [22]. The ionization potential $U_i = 12.1 \text{ eV}$, and the neutral oxygen density $\rho_{nt} = 5.4 \times 10^{18} \text{ cm}^{-3}$. $\mathcal{R}(t-t')$ is the nonlinear Kerr response including a Raman-delayed contribution [23]. Due to the weak dependence of the nonlinear refractive index on the wavelength [24], we adopt a fixed value $n_2 = 1.3 \times 10^{-19} \text{ cm}^2/\text{W}$ [25]. To perform (3D+1) simulations, we first obtain the nonlinear envelope equation in the spectral domain (k_x, k_y, ω) by a spatial and temporal Fourier transform. This equation is an ordinary differential equation for a spectral amplitude with the differential variable z . We solve the equation iteratively using the implicit finite-difference method. The obtained spectral amplitude is then transformed to the spatiotemporal domain (x, y, t) by an inverse Fourier transform [26]. The spatial and temporal resolutions used in our simulations are $20 \mu\text{m}$ and 0.5 fs , respectively. The input laser pulse has a Gaussian spatiotemporal distribution with a temporal duration (FWHM) τ_0 , and a beam waist $2w_0 = 2 \text{ mm}$, focused by a lens with $f = 1 \text{ m}$. The input peak power is $P_{in} = 4P_{cr}$, where the critical power for self-focusing is $P_{cr} = 3.77\lambda_0^2/8\pi n_2$ [27]. The random noise with an amplitude of 10% is added to the input electric field envelope.

III. RESULTS AND DISCUSSION

We start with the case when $\lambda_0 = 1.5 \mu\text{m}$ and $\tau_0 = 50 \text{ fs}$. Figure 1(a) shows the peak intensity evolution of the $1.5\text{-}\mu\text{m}$ pulse propagating in the air and air-plasma channel with the required electron density $\rho_p = 8.8 \times 10^{16} \text{ cm}^{-3}$ predicted by Eq. (2). For the propagation in air, as the pulse self-focuses, the intensity increases rapidly and then is clamped at 60 TW/cm^2 . Accordingly, the electron density generated by the pulse is increased to $7 \times 10^{15} \text{ cm}^{-3}$. As a result, the pulse splits at $z = 0.8 \text{ m}$ due to plasma defocusing and subsequent refocusing of the pulse trailing edge, as shown in Fig. 1(b). Here, the defocusing is caused by the electrons generated by the pulse itself because of the nonuniform distribution in the transverse plane. With the diffraction of the subpulses, the filamentation is terminated at about $z = 2 \text{ m}$. The filament is prolonged more than threefold when there is a preformed plasma channel [Fig. 1(c)]. In this case, the filamentation process is divided into two stages at $z = 1.7 \text{ m}$. In the first stage, the intensity evolution is similar to that without a preformed plasma channel, with a clamping intensity $\sim 60 \text{ TW/cm}^2$. In the beginning of the second stage, the intensity first decreases due to pulse splitting and then increases again due to the coalescence of subpulses. The coalescence of subpulses can enrich the spectrum, making it able to support a shorter pulse. Then the intensity is clamped at $\sim 70 \text{ TW/cm}^2$ from $z = 2$ to 6 m . At this stage, a stable temporal profile is

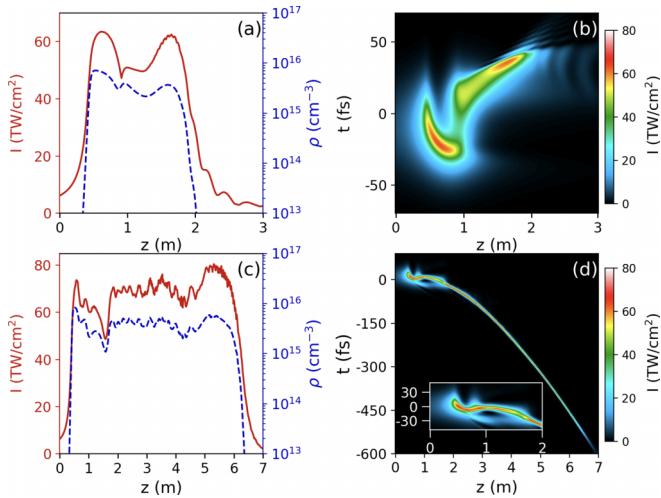


FIG. 1. (a), (c) Peak intensity (solid lines) of the femtosecond pulse and the peak density of electron generated by the femtosecond pulse (dashed lines) as a function of propagation distance, when the 1.5- μm pulse propagates in the (a) air and (c) air-plasma channel with $\rho_0 = 8.8 \times 10^{16} \text{ cm}^{-3}$. (b), (d) On-axis pulse evolution when propagating in the (b) air and (d) air-plasma channel.

observed [Fig. 1(d)]. Combined with the spatial characteristics of filamentation, the long-distance STS is generated as we expect.

To observe the detailed propagation of STS and confirm its self-cleaning, in Fig. 2 we plot the spatiotemporal intensity distribution of the pulse at several propagation distances. At $z = 0.5 \text{ m}$, the pulse trailing edge is defocused by the plasma generated at the leading edge, leading to a fishbone structure in the intensity distribution. After pulse splitting at $z = 1 \text{ m}$, the rear subpulse with a higher frequency starts to catch up with the front pulse. Consequently, the coalescence of the two subpulses occurs at $z = 1.6 \text{ m}$. The isolated pulse with a duration of 22 fs is further compressed to 8 fs at $z = 2 \text{ m}$. At the initial stage of the soliton regime, there are sidelobes both before and after the main pulse. We find that both ionization and long-distance propagation play important roles in eliminating these sidelobes. Although STS has been observed in fused silica [28], there is no significant improvement of temporal quality due to the short propagation distance. As shown in Fig. 3(c), the carrier wavelength continuously shifts towards the blue side due to ionization. As a result, the main pulse with a larger group velocity captures the front sidelobes. Meanwhile, the power that the latter sidelobes possess is insufficient to overcome plasma defocusing, thus they are gradually dissipated to the off-axis region. Therefore, the sidelobes are eliminated and the temporal profile of the few-cycle pulse is self-cleaned after a long-distance propagation.

The output pulse profile at $z = 6 \text{ m}$, integrated over a circular region with 200 μm radius, is shown in Fig. 3(a). The pulse duration is 5.3 fs, indicating a compression factor close to 10.

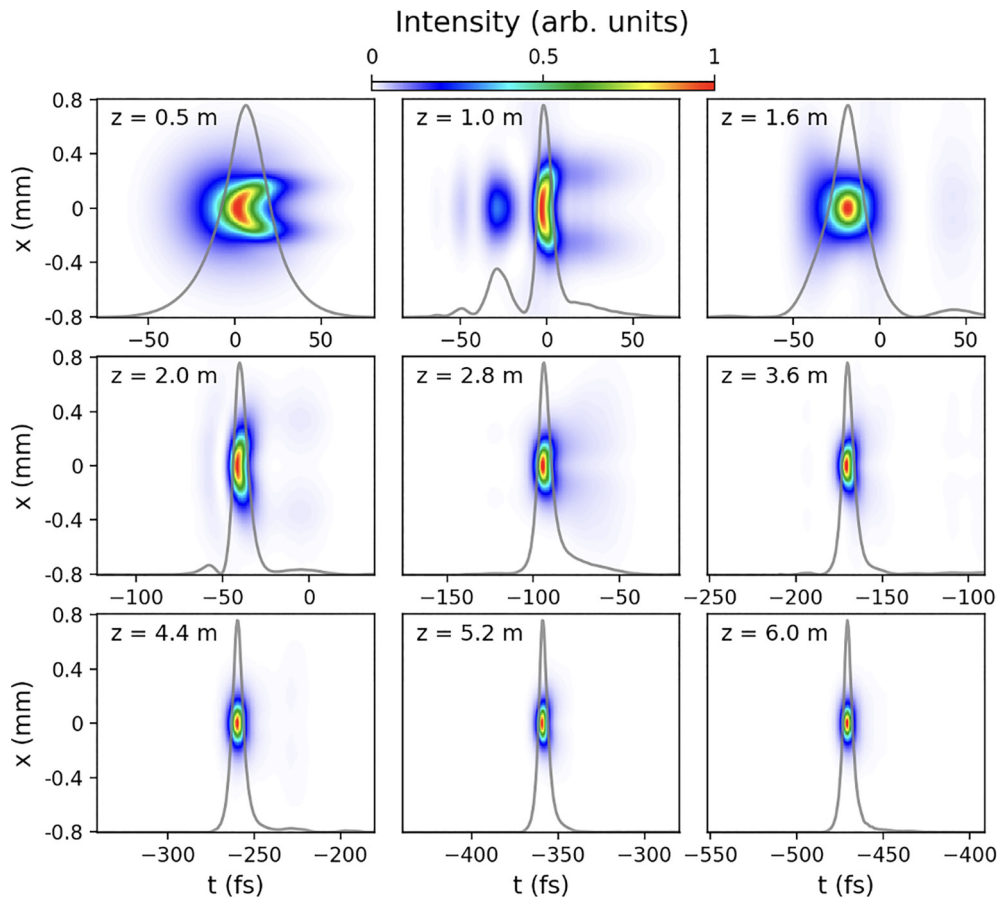


FIG. 2. Normalized spatiotemporal intensity evolution for $\lambda_0 = 1.5 \mu\text{m}$, $\tau_0 = 50 \text{ fs}$, $\rho_0 = 8.8 \times 10^{16} \text{ cm}^{-3}$. The temporal profiles integrated over a circular region with 200 μm radius are marked on the graph.

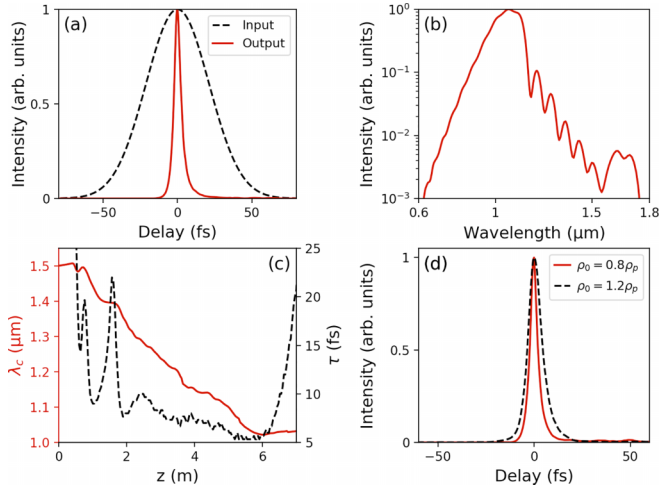


FIG. 3. (a) Output pulse profile and (b) spectrum at $z = 6$ m when $\rho_0 = \rho_p = 8.8 \times 10^{16} \text{ cm}^{-3}$, and the intensity is integrated over a circular region with $200 \mu\text{m}$ radius. (c) The evolution of carrier wavelength λ_c (solid line) and the pulse duration τ (dashed line). (d) Output pulses when employing air-plasma channels with $\rho_0 = 0.8\rho_p$ (solid line) and $\rho_0 = 1.2\rho_p$ (dashed line).

More importantly, the sub-two-cycle pulse has a clean pulse shape without accompanying sidelobes. The corresponding spectrum spans more than an octave, with the carrier wavelength shifted to $\sim 1.1 \mu\text{m}$ due to ionization [Fig. 3(b)]. The blueshift of the carrier wavelength is beneficial to acquiring shorter pulse. In Fig. 3(c) we plot the evolution curves of the carrier wavelength $\lambda_c = \int_0^\infty I(\lambda)\lambda d\lambda / \int_0^\infty I(\lambda) d\lambda$ and pulse duration. At the soliton stage (after $z = 2$ m), the carrier wavelength decreases with almost a fixed rate, and the pulse duration also decreases. This can be understood by the self-organization behavior of the soliton. In order to maintain equilibrium between the Kerr effect and dispersion, the soliton will continue self-compression to compensate for the energy dissipation caused by ionization. When the soliton cannot be sustained (after $z = 6$ m), the laser intensity drops, and the pulse is stretched rapidly. Note that due to the self-organization of STS, its formation and self-cleaning are not sensitive to parameters such as other methods. Figure 3(d) shows the output pulse profiles when there is a 20% deviation of the plasma density. When $\rho_0 = 0.8\rho_p$, the pulse is compressed to 4.3 fs, with only a very weak sidelobe after the main pulse, which results from the shortened soliton propagation length. When $\rho_0 = 1.2\rho_p$, there is no sidelobe, and the pulse duration is slightly larger (8.2 fs). This is because for stronger dispersion, only a relatively large pulse duration can maintain the stability of the soliton, which is also consistent with the temporal soliton solution in Ref. [29].

We also investigate the pulse self-compression for different input laser powers. Figure 4 shows the output pulse durations when P_{in} changes from $2P_{\text{cr}}$ to $10P_{\text{cr}}$. The filament length, defined as the propagation distance that the maximum intensity is larger than 30 TW/cm^2 , is given in the same plot. When $P_{\text{in}} < 4P_{\text{cr}}$, the spectrum is not wide enough after pulse splitting, and the subpulses cannot fully coalesce before intensity drops. No STS is formed and the filament length is only ~ 1 m. Therefore, the output pulse duration is larger, and sidelobes

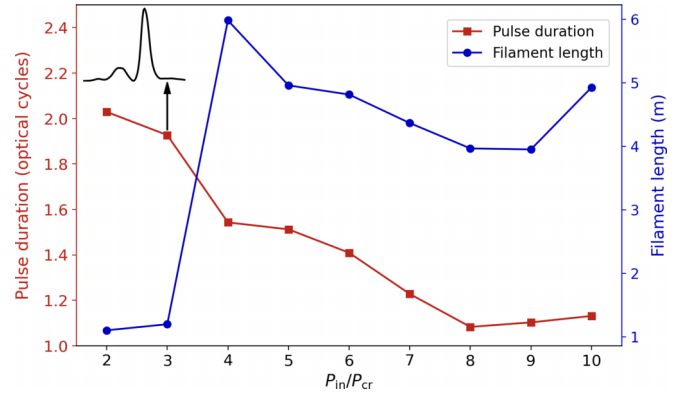


FIG. 4. The output pulse duration and filament length as a function of input power. The pulse duration is in the unit of optical cycles, and ρ_0 is fixed at $8.8 \times 10^{16} \text{ cm}^{-3}$. The inset shows the output pulse profile when $P_{\text{in}} = 3P_{\text{cr}}$.

are observed. For $P_{\text{in}} = 4P_{\text{cr}}$, the filament length is significantly extended. In this case, long-distance STS eliminates temporal sidelobes of the pulse as discussed before. As P_{in} increases from $4P_{\text{cr}}$ to $8P_{\text{cr}}$, the filament length remains in the range 4–5 m, and the output pulse duration slightly decreases, close to the single-cycle regime. This is because for a higher input power, plasma defocusing is stronger before pulse splitting. Then at the refocusing stage, the spatiotemporal focusing effect leads to a higher clamping intensity and thus a broader spectrum. Further increasing P_{in} can no longer increase the clamping intensity. Therefore, the pulse duration is limited to the single-cycle regime. Moreover, simply increasing the input power cannot significantly increase the output peak power ($\sim 50 \text{ GW}$) due to intensity clamping and soliton size limitation. Note that we do not observe multiple filament formation even when $P_{\text{in}} = 10P_{\text{cr}}$ and 10% random noise is introduced to the initial amplitude. The reason is twofold. On the one hand, our input beam size is small, which is resistant to multifilamentation [30]. On the other hand, the strong GVD could counter the Kerr self-focusing and increase the effective critical power [31,32], which also inhibits the formation of multiple filaments.

Since the STS results from the interplay of nonlinear effects and GVD, our scheme should be applicable to pulses with different central wavelengths by properly modulating the dispersion relation of air. As a check on this, we tested our scheme for 0.8- and 3- μm pulses. The input pulse durations are 25 fs for $\lambda_0 = 0.8 \mu\text{m}$ and 80 fs for $\lambda_0 = 3 \mu\text{m}$, and the input power is kept at $P_{\text{in}} = 4P_{\text{cr}}$. Using the predicted values of plasma density from Eq. (2), $\rho_p = 2.9 \times 10^{17}$ and $1.4 \times 10^{16} \text{ cm}^{-3}$, respectively, we successfully obtain sub-two-cycle pulses with a high temporal quality, as shown in Fig. 5. The output pulse profiles are integrated over circular regions with radius $r_0 = 100 \mu\text{m}$ for $\lambda_0 = 0.8 \mu\text{m}$ and $r_0 = 600 \mu\text{m}$ for $\lambda_0 = 3 \mu\text{m}$, giving pulse durations of 3.7 and 17.3 fs, both shorter than two optical cycles. Similar STS is also observed in the spatiotemporal intensity distribution (insets of Fig. 5), which further confirms that our scheme can be applied to generate few-cycle pulses with a desired wavelength.

Future experimental verifications may be achieved by filamentation of high-energy picosecond laser beams [27,33].

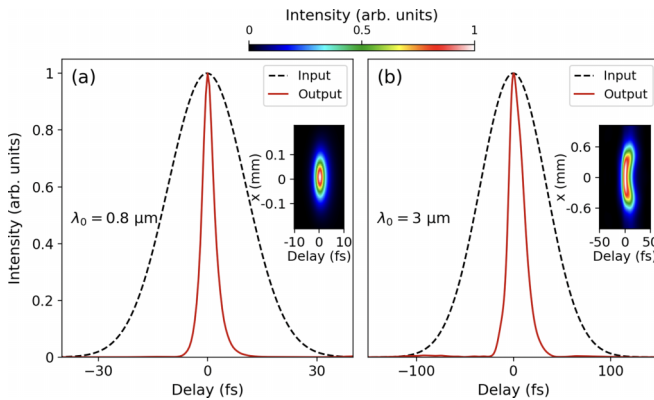


FIG. 5. Input (dashed lines) and output (solid lines) pulse shapes when applying the plasma compression scheme to (a) near-infrared and (b) midinfrared laser pulses. Simulation parameters: (a) $\lambda_0 = 0.8 \mu\text{m}$, $\rho_0 = 2.9 \times 10^{17} \text{cm}^{-3}$, $\tau_0 = 25 \text{fs}$; (b) $\lambda_0 = 3 \mu\text{m}$, $\rho_0 = 1.4 \times 10^{16} \text{cm}^{-3}$, $\tau_0 = 80 \text{fs}$. The input peak power is $P_{\text{in}} = 4P_{\text{cr}}$. The output pulse durations are integrated over circular regions with radius (a) $r_0 = 100 \mu\text{m}$ and (b) $r_0 = 600 \mu\text{m}$. The insets show the normalized spatiotemporal intensity distribution.

In Ref. [27], a 5-m-long air-plasma channel with a diameter of approximately 1 cm was successfully generated, and the plasma density is around 10^{15}cm^{-3} . With the development of picosecond laser technology, it is possible that the required

parameters for the plasma channel in our simulations could be achieved. Perhaps achieving a perfectly uniform density distribution experimentally is challenging. However, a small density fluctuation will not affect the self-cleaning process of spatiotemporal solitons, as indicated by our simulation results.

IV. CONCLUSION

In summary, we have proposed a scheme for generating sub-two-cycle pulses with a high temporal quality by self-compression of femtosecond pulses in preformed uniform air-plasma channels. Plasma-induced negative dispersion enables the generation of a long-distance spatiotemporal soliton, which leads to continuous pulse self-cleaning and the elimination of temporal sidelobes. By changing the density of preformed air-plasma channels, this scheme can be applied to compress femtosecond laser pulses with different central wavelengths to sub-two-cycle pulses with a high temporal quality. Such versatility, together with the robustness of our scheme, should greatly facilitate wavelength-dependent applications of few-cycle pulses in ultrafast science.

ACKNOWLEDGMENTS

The authors would like to thank Prof. J. Zhang of Shanghai Jiao Tong University for fruitful suggestions. This work was supported by the National Natural Science Foundation of China (Grants No. 11874056, No. 12074228, and No. 11774038).

- [1] F. Siegrist, J. A. Gessner, M. Ossiander, C. Denker, Y.-P. Chang, M. C. Schröder, A. Guggenmos, Y. Cui, J. Walowski, U. Martens, J. K. Dewhurst, U. Kleineberg, M. Münzenberg, S. Sharma, and M. Schultze, Light-wave dynamic control of magnetism, *Nature (London)* **571**, 240 (2019).
- [2] F. Calegari, D. Ayuso, A. Trabattori, L. Belshaw, S. De Camillis, S. Anumula, F. Frassetto, L. Poletto, A. Palacios, P. Decleva, J. B. Greenwood, F. Martín, and M. Nisoli, Ultrafast electron dynamics in phenylalanine initiated by attosecond pulses, *Science* **346**, 336 (2014).
- [3] G. Sansone, E. Benedetti, F. Calegari, C. Vozzi, L. Avaldi, R. Flammini, L. Poletto, P. Villoresi, C. Altucci, R. Velotta, S. Stagira, S. De Silvestri, and M. Nisoli, Isolated single-cycle attosecond pulses, *Science* **314**, 443 (2006).
- [4] Y. Shou, R. Hu, Z. Gong, J. Yu, J. E. Chen, G. Mourou, X. Yan, and W. Ma, Cascaded generation of isolated sub-10 attosecond half-cycle pulses, *New J. Phys.* **23**, 053003 (2021).
- [5] X. Z. Wu, Z. Gong, Y. R. Shou, Y. H. Tang, J. Q. Yu, G. Mourou, and X. Q. Yan, Efficiency enhancement of ion acceleration from thin target irradiated by multi-PW few-cycle laser pulses, *Phys. Plasmas* **28**, 023102 (2021).
- [6] X. F. Shen, B. Qiao, H. Zhang, Y. Xie, S. Kar, M. Borghesi, M. Zepf, C. T. Zhou, S. P. Zhu, and X. T. He, Electrostatic capacitance-type acceleration of ions with an intense few-cycle laser pulse, *Appl. Phys. Lett.* **114**, 144102 (2019).
- [7] M. Seo, K. Tsendsuren, S. Mitra, M. Kling, and D. Kim, High-contrast, intense single-cycle pulses from an all thin-solid-plate setup, *Opt. Lett.* **45**, 367 (2020).
- [8] M. Ouillé, A. Vernier, F. Böhle, M. Bocoum, A. Jullien, M. Lozano, J.-P. Rousseau, Z. Cheng, D. Gustas, A. Blumenstein, P. Simon, S. Haessler, J. Faure, T. Nagy, and R. Lopez-Martens, Relativistic-intensity near-single-cycle light waveforms at kHz repetition rate, *Light: Sci. Appl.* **9**, 47 (2020).
- [9] S. Akturk, A. Couairon, M. Franco, and A. Mysyrowicz, Spectrogram representation of pulse self-compression by filamentation, *Opt. Express* **16**, 17626 (2008).
- [10] H. Timmers, Y. Kobayashi, K. F. Chang, M. Reduzzi, D. M. Neumark, and S. R. Leone, Generating high-contrast, near single-cycle waveforms with third-order dispersion compensation, *Opt. Lett.* **42**, 811 (2017).
- [11] A. Couairon, M. Franco, A. Mysyrowicz, J. Biegert, and U. Keller, Pulse self-compression to the single-cycle limit by filamentation in a gas with a pressure gradient, *Opt. Lett.* **30**, 2657 (2005).
- [12] C. Brée, J. Bethge, S. Skupin, L. Bergé, A. Demircan, and G. Steinmeyer, Cascaded self-compression of femtosecond pulses in filaments, *New J. Phys.* **12**, 093046 (2010).
- [13] T. Balciunas, C. Fourcade-Dutin, G. Fan, T. Witting, A. A. Voronin, A. M. Zheltikov, F. Jerome, G. G. Paulus, A. Baltuska, and F. Benabid, A strong-field driver in the single-cycle regime based on self-compression in a kagome fibre, *Nat. Commun.* **6**, 6117 (2015).
- [14] W. Liu and S. L. Chin, Abnormal wavelength dependence of the self-cleaning phenomenon during femtosecond-laser-pulse filamentation, *Phys. Rev. A* **76**, 013826 (2007).

- [15] I. Koprnikov, Ionization variation of the group velocity dispersion by high-intensity optical pulses, *Appl. Phys. B* **79**, 359 (2004).
- [16] C. Finot, F. Chaussard, and S. Boscolo, Simple guidelines to predict self-phase modulation patterns, *J. Opt. Soc. Am. B* **35**, 3143 (2018).
- [17] Y.-C. Cheng, C.-H. Lu, Y.-Y. Lin, and A. H. Kung, Supercontinuum generation in a multi-plate medium, *Opt. Express* **24**, 7224 (2016).
- [18] A. Couairon and A. Mysyrowicz, Femtosecond filamentation in transparent media, *Phys. Rep.* **441**, 47 (2007).
- [19] S. Champeaux and L. Bergé, Postionization regimes of femtosecond laser pulses self-channeling in air, *Phys. Rev. E* **71**, 046604 (2005).
- [20] J. Zhang, Z. H. Lu, and L. J. Wang, Precision refractive index measurements of air, N₂, O₂, Ar, and CO₂ with a frequency comb, *Appl. Opt.* **47**, 3143 (2008).
- [21] R. J. Mathar, Refractive index of humid air in the infrared: Model fits, *J. Opt. A: Pure Appl. Opt.* **9**, 470 (2007).
- [22] A. M. Perelomov, V. S. Popov, and M. V. Terent'ev, Ionization of atoms in an alternating electric field, *Zh. Eksp. Teor. Fiz.* **50**, 1393 (1966) [*Sov. Phys. JETP* **23**, 924 (1966)].
- [23] L. Bergé, S. Skupin, and G. Steinmeyer, Temporal self-restoration of compressed optical filaments, *Phys. Rev. Lett.* **101**, 213901 (2008).
- [24] S. Zahedpour, J. K. Wahlstrand, and H. M. Milchberg, Measurement of the nonlinear refractive index of air constituents at mid-infrared wavelengths, *Opt. Lett.* **40**, 5794 (2015).
- [25] L. Bergé, Self-compression of 2 μm laser filaments, *Opt. Express* **16**, 21529 (2008).
- [26] A. Couairon, E. Brambilla, T. Corti, D. Majus, O. de J. Ramírez-Góngora, and M. Kolesik, Practitioner's guide to laser pulse propagation models and simulation: Numerical implementation and practical usage of modern pulse propagation models, *Eur. Phys. J.: Spec. Top.* **199**, 5 (2011).
- [27] S. Tochitsky, E. Welch, M. Polyanskiy, I. Pogorelsky, P. Panagiotopoulos, M. Kolesik, E. M. Wright, S. W. Koch, J. V. Moloney, J. Pigeon, and C. Joshi, Megafilament in air formed by self-guided terawatt long-wavelength infrared laser, *Nat. Photon.* **13**, 41 (2019).
- [28] M. Durand, A. Jarnac, A. Houard, Y. Liu, S. Grabielle, N. Forget, A. Durécu, A. Couairon, and A. Mysyrowicz, Self-guided propagation of ultrashort laser pulses in the anomalous dispersion region of transparent solids: A new regime of filamentation, *Phys. Rev. Lett.* **110**, 115003 (2013).
- [29] N. Tzoar and M. Jain, Self-phase modulation in long-geometry optical waveguides, *Phys. Rev. A* **23**, 1266 (1981).
- [30] R. I. Grynko, D. L. Weerawarne, X. Gao, H. Liang, H. J. Meyer, K.-H. Hong, A. L. Gaeta, and B. Shim, Inhibition of multi-filamentation of high-power laser beams, *Opt. Lett.* **41**, 4064 (2016).
- [31] S.-Y. Li, F.-M. Guo, Y. Song, A.-M. Chen, Y.-J. Yang, and M.-X. Jin, Influence of group-velocity-dispersion effects on the propagation of femtosecond laser pulses in air at different pressures, *Phys. Rev. A* **89**, 023809 (2014).
- [32] S. Skupin, R. Nuter, and L. Bergé, Optical femtosecond filaments in condensed media, *Phys. Rev. A* **74**, 043813 (2006).
- [33] A. Schmitt-Sody, H. G. Kurz, L. Bergé, S. Skupin, and P. Polynkin, Picosecond laser filamentation in air, *New J. Phys.* **18**, 093005 (2016).